

Magnetotransport of a 2DEG with anisotropic Rashba interaction at the LaAlO₃/SrTiO₃ interface

Azadeh Faridi,^{1,2} Reza Asgari,^{2,3,*} and Abdollah Langari^{1,2}

¹*Department of Physics, Sharif University of Technology, Tehran, Iran*

²*School of Physics, Institute for Research in Fundamental Sciences (IPM), Tehran 19395-5531, Iran*

³*School of Nano Science, Institute for Research in Fundamental Sciences (IPM), Tehran 19395-5531, Iran*

(Dated: June 27, 2021)

We investigate the magnetotransport properties of a two-dimensional electron gas with anisotropic k -cubic Rashba interaction at the LaAlO₃/SrTiO₃ interface. The Landau levels and density of states of the system as well as the magnetotransport coefficients are evaluated. A somehow anomalous beating pattern in low magnetic field regime is found both in the density profile and magnetoresistivity. We discuss the impact of electron density, Landau level broadening and Rashba spin-orbit constant on the appearance of the beatings in low magnetic fields and find that at low electron concentrations and not very strong spin-orbit interactions the beatings smooth out. On the other hand, as the magnetic field increases, the Zeeman term becomes the dominant splitting mechanism leading to the spin-split peaks in SdH oscillations. We also show that the observation of the beatings in low magnetic fields needs a system with rather higher carrier concentration so that the beatings persist up to sufficiently large fields where the oscillations are not smoothed out by Landau level broadening. The quantum Hall plateaus are evaluated and we show the Chern number with both even and odd values is replaced by the odd numbers when two subband energies are close with spin degenerate energy levels. Along with the numerical evaluation of the magnetotransport properties, a perturbative calculation is also performed which can be used in the case of low densities and not very large filling factors.

PACS numbers: 73.20.Mf, 73.21.Ac, 68.65.Pq

I. INTRODUCTION

The two-dimensional electron gas (2DEG) formed at the interface of two band insulators LaAlO₃ and SrTiO₃ has been the subject of various research topics such as metal-insulator phase transition [1], tunable spin-orbit coupling [2], magnetism [3], superconductivity [4] and their coexistence [5] to name some [6]. Quantum oscillations in the form of Shubnikov-de Haas (SdH) oscillations have also been observed in this system underlying the two dimensional character of the electronic states [7–11]. Although there are several experimental reports on SdH oscillations in this system, we have not achieved yet a unique picture of the quantum transport at the interface owing to variable samples studied and also different conditions under which the experiments have been performed. Moreover, large effective mass of the carriers at oxide interfaces compared to their semiconductor counterparts results in smaller Landau level separation and thus together with rather lower mobility of carriers in this case cause a challenging situation for observation of quantum conductance. By the same token, the realization of the quantum Hall effect (QHE) has been elusive in this system. The lack of relatively high mobility samples with sufficiently low carrier densities have hindered the observation of the QHE especially at lower filling factors. Therefore there have been so far a few and very diverse reports of observation of somehow imperfect

plateaus of Hall conductance only in higher filling factors [11–13]. It is worthwhile mentioning that in most reported SdH experiments, the carrier concentration is smaller than the carrier concentration obtained from the Hall effect. The possible reasoning is that there may exist carriers with low mobility due to the diffusive scattering process and would be difficult to observe them in SdH experiment [14].

The host of the 2DEG residing at the interface of LaAlO₃ and SrTiO₃ are the t_{2g} orbitals of Ti atom [15, 16]. Due to the confinement of the electron gas along \hat{z} , d_{xy} orbital has a lower energy than d_{xz} and d_{yz} orbitals. Furthermore, while d_{xy} orbital forms an isotropic band with the same light mass in both \hat{x} and \hat{y} , the d_{xz} and d_{yz} orbitals have a light effective mass in \hat{x} (\hat{y}) and a heavy effective mass along \hat{y} (\hat{x}) forming anisotropic bands. The inversion symmetry breaking along \hat{z} at the interface together with the atomic spin-orbit interaction also result in a Rashba spin splitting as well as the orbital mixing of the bands [17, 18]. Following a quasi-degenerate perturbation approach Zhou *et al* developed an effective Hamiltonian around Γ point suggesting the usual k -linear Rashba spin-orbit coupling for d_{xy} orbital but an anisotropic k -cubic spin-orbit interaction for d_{xz} and d_{yz} orbitals [19]. The same theoretical results were found by several groups as well [18, 20, 21]. The possibility of the k -cubic Rashba spin splitting was also reported experimentally [22, 23]. On the other hand, some magnetotransport experiments suggest that the SdH oscillations in this system originate from the carriers with rather heavy effective mass illustrating the dominant con-

* asgari@ipm.ir

tribution of d_{xz} and d_{yz} orbitals in quantum oscillations [9, 10]. This is attributed to the spatial extension of these orbitals deeper into the SrTiO₃ (in comparison with closer-to-interface d_{xy} orbital) so that they experience less scatterings due to disorders or lattice distortions and as a result these carriers have a high enough mobility to show the quantum oscillations.

Accordingly in this work, in order to find the magnetotransport properties of the system, we begin with the effective two-band Hamiltonian of anisotropic d_{xz}/d_{yz} orbitals with k -cubic Rashba spin-orbit coupling [19] and study the system in the presence of a magnetic field perpendicular to the interface. The Landau levels, as well as the chemical potential and density of states of the system, are found and we continue with the evaluation of the magnetotransport coefficients of the system. A rather anomalous beating pattern (due to the presence of the anisotropic k -cubic Rashba spin-orbit interaction in the Hamiltonian) is found in lower magnetic fields or larger filling factors. For larger magnetic fields, the Zeeman term becomes the dominant spin splitting mechanism so that the split conductivity peaks appear in longitudinal conductivity curves. The effects of the carrier density, Rashba strength, and Landau level broadening are also discussed and we show that in a system with rather lower carrier concentrations, the beatings are expected to appear in such a low magnetic field region where level broadenings due to disorder or temperature can even fully spoil the beating pattern.

The paper is organized as follows. In Sec. II, the eigenvalues and eigenfunctions of the system under magnetic field along \hat{z} are found both numerically and analytically (for weak Rashba interaction). The chemical potential and density of the system are also evaluated in this section. Next in Sec. III, the expressions of both longitudinal and Hall conductivities derived from a linear-response-based formalism are introduced and discussed for our system. The numerical results of these two sections are presented in Sec. IV together with the results of the de-Haas van Alphen oscillations of magnetization and finally the results are summarized in Sec. V.

II. BASIC FORMULATION

We consider the effective Hamiltonian introduced in Ref. 19 for a pair of bands which is a hybridization of d_{xz} and d_{yz} orbitals, subject to a magnetic field along \hat{z}

$$\mathcal{H} = \Pi^2/2m^* + \frac{\alpha_0}{2\hbar^3} \{(\Pi_-^2 + \Pi_+^2), (\Pi \times \sigma)_z\} + \frac{1}{2}g\mu_B B\sigma_z, \quad (1)$$

where α_0 is the strength of the cubic spin-orbit interaction, $\Pi = \mathbf{p} + e\mathbf{A}$ is the canonical momentum with \mathbf{p} the momentum operator and \mathbf{A} the vector potential, $\Pi_{\pm} = \Pi_x \pm i\Pi_y$, g is the effective Zeeman factor, and μ_B is the Bohr magneton. We also define $\{A, B\} = (AB + BA)/2$. In order to find Landau levels of the system in Lan-

dau gauge $\mathbf{A} = (0, Bx, 0)$, we introduce the creation and annihilation operators $a = \sqrt{\frac{1}{2\hbar m^* \omega_c}}(\Pi_y + i\Pi_x)$ and $a^\dagger = \sqrt{\frac{1}{2\hbar m^* \omega_c}}(\Pi_y - i\Pi_x)$ where $\omega_c = \frac{eB}{m^*}$ is the cyclotron frequency, $\Pi_x = p_x$ and $\Pi_y = p_y + m^* \omega_c x$ and m^* is the band effective mass. Rewriting the Hamiltonian using these operators, we will have $\mathcal{H} = H_0 + H_1 + H_2$ with

$$H_0 = \hbar\omega_c \begin{pmatrix} (1/2 + a^\dagger a) + \xi & 0 \\ 0 & (1/2 + a^\dagger a) - \xi \end{pmatrix}, \quad (2)$$

$$H_1 = \alpha \begin{pmatrix} 0 & a^\dagger a a^\dagger \\ a a^\dagger a & 0 \end{pmatrix}, \quad (3)$$

$$H_2 = \alpha \begin{pmatrix} 0 & a^3 \\ a^{\dagger 3} & 0 \end{pmatrix}, \quad (4)$$

where $\xi = g\mu_B m^*/2e\hbar = gm^*/4m_e$, $\alpha = \frac{\alpha_0}{2\hbar^3} (2\hbar\omega_c m^*)^{3/2}$ and m_e is the electron rest mass. The general way to solve eigenvalue equation $(\mathcal{H} - EI)\Psi = 0$ is to expand the eigenvectors of the system in harmonic oscillator functions as

$$\begin{aligned} \Psi &= \frac{e^{ik_y y}}{\sqrt{L_y}} \left(\sum_n C_n^\uparrow \phi_n(x - x_c) \right. \\ &\quad \left. + \sum_n C_n^\downarrow \phi_n(x - x_c) \right) \\ &= \frac{e^{ik_y y}}{\sqrt{L_y}} \sum_n [C_n^\uparrow \phi_n(x - x_c) |\uparrow\rangle + C_n^\downarrow \phi_n(x - x_c) |\downarrow\rangle], \end{aligned} \quad (5)$$

Here n is the Landau level index, L_y is the length of the system along the y direction, $\phi_n(x - x_c) = e^{-(x-x_c)^2/2l_c^2} H_n[(x-x_c)/l_c]/\sqrt{\sqrt{\pi} l_c 2^n n!}$ is the harmonic oscillator state with $H_n[(x-x_c)/l_c]$ the Hermite polynomial of order n , $l_c = \sqrt{\hbar/m^* \omega_c}$ is the magnetic length, $x_c = l_c^2 k_y$ is the center of oscillation and $|\uparrow\rangle$ ($|\downarrow\rangle$) is the spinor related to spin up (down).

To get more insight to the problem, it would be useful to look at cases when we have only H_1 or H_2 term. It is interesting to note that H_1 is very similar to linear Rashba spin-orbit interaction [24, 25], because it also couples two Landau levels of the order n and $n-1$ with opposite spins. Solving eigenvalue problem for $\mathcal{H} = H_0 + H_1$, the Landau levels would be

$$E_n^s = \hbar\omega_c n + s\hbar\omega_c (1/2 + \xi) \sqrt{1 + \frac{4\alpha^2 n^3}{\hbar^2 \omega_c^2 (1 + 2\xi)^2}}, \quad (6)$$

with $s = +1$ for spin up and $s = -1$ for spin down. The eigenfunctions are given by

$$\psi_n^+ = \frac{e^{ik_y y}}{\sqrt{L_y}} [\cos \theta_n \phi_n |\uparrow\rangle + \sin \theta_n \phi_{n-1} |\downarrow\rangle], \quad (7)$$

$$\psi_n^- = \frac{e^{ik_y y}}{\sqrt{L_y}} [-\sin \theta_n \phi_n |\uparrow\rangle + \cos \theta_n \phi_{n-1} |\downarrow\rangle], \quad (8)$$

for $n = 1, 2, 3, \dots$. We have defined θ_n such that $\tan(\theta_n) = 2\alpha n^{3/2}/(\delta + \delta\sqrt{1 + 4\alpha^2 n^3/\delta^2})$, where $\delta = \hbar\omega_c(1 + 2\xi)$. It can be seen that H_1 couples state $\phi_n |\uparrow\rangle$ with $\phi_{n-1} |\downarrow\rangle$. The only state that remains unchanged is the lowest spin up Landau level $\psi_0^+ = \frac{e^{ik_y y}}{\sqrt{L_y}} \phi_0 |\uparrow\rangle$ with eigenvalue $E_0^+ = \hbar\omega_c(1/2 + \xi)$.

On the other hand, $\mathcal{H} = H_0 + H_2$ is exactly the Hamiltonian of a system with isotropic cubic Rashba interaction which had been suggested for hole gas systems [26, 27]. In this case, the eigenvalues are

$$E_n^s = \hbar\omega_c(n-1) + s\hbar\omega_c(3/2 - \xi) \sqrt{1 + \frac{\alpha^2 n(n-1)(n-2)}{\hbar^2 \omega_c^2 (3/2 - \xi)^2}}, \quad (9)$$

with eigenfunctions

$$\psi_n^+ = \frac{e^{ik_y y}}{\sqrt{L_y}} [\sin \theta_n \phi_{n-3} |\uparrow\rangle + \cos \theta_n \phi_n |\downarrow\rangle], \quad (10)$$

$$\psi_n^- = \frac{e^{ik_y y}}{\sqrt{L_y}} [\cos \theta_n \phi_{n-3} |\uparrow\rangle - \sin \theta_n \phi_n |\downarrow\rangle], \quad (11)$$

for $n = 3, 4, 5, \dots$, where $\tan(\theta_n) = \alpha\sqrt{n(n-1)(n-2)}/(\delta + \delta\sqrt{1 + \alpha^2 n(n-1)(n-2)/\delta^2})$ and $\delta = \hbar\omega_c(3/2 - \xi)$. It is clear that H_2 mixes every $\phi_n |\uparrow\rangle$ with $\phi_{n+3} |\downarrow\rangle$. Again, we have three states $n = 0, 1, 2$, which do not couple with other states, i.e. eigenvalues $E_n^- = \hbar\omega_c(n+1/2) - \hbar\omega_c\xi$ and eigenfunctions $\psi_n^- = \frac{e^{ik_y y}}{\sqrt{L_y}} \phi_n |\downarrow\rangle$. Therefore, for $n = 0, 1, 2$ we do not have any + branch.

When both H_1 and H_2 are present, the Hamiltonian should be diagonalized numerically in a truncated Hilbert space with the sufficiently large number of basis functions. We can see that in this case, the Landau levels of the system fall into the following four groups with different couplings

$$\phi_0 |\downarrow\rangle \xrightarrow{H_1} \phi_1 |\uparrow\rangle \xrightarrow{H_2} \phi_4 |\downarrow\rangle \xrightarrow{H_1} \phi_5 |\uparrow\rangle \xrightarrow{H_2} + \dots, (I)$$

$$\phi_1 |\downarrow\rangle \xrightarrow{H_1} \phi_2 |\uparrow\rangle \xrightarrow{H_2} \phi_5 |\downarrow\rangle \xrightarrow{H_1} \phi_6 |\uparrow\rangle \xrightarrow{H_2} + \dots, (II)$$

$$\phi_2 |\downarrow\rangle \xrightarrow{H_1} \phi_3 |\uparrow\rangle \xrightarrow{H_2} \phi_6 |\downarrow\rangle \xrightarrow{H_1} \phi_7 |\uparrow\rangle \xrightarrow{H_2} + \dots, (III)$$

$$\phi_0 |\uparrow\rangle \xrightarrow{H_2} \phi_3 |\downarrow\rangle \xrightarrow{H_1} \phi_4 |\uparrow\rangle \xrightarrow{H_2} \phi_7 |\downarrow\rangle \xrightarrow{H_1} + \dots, (IV)$$

On the other hand, because of the large value of the Zeeman term with respect to the Rashba interaction, we can find an approximate solution to this problem treating both H_1 and H_2 as perturbations to H_0 . Therefore, to the second order of perturbations the Landau levels are

$$E_n^+ = E_n^{0+} + \frac{\alpha^2 n^3}{(1 + 2\xi)\hbar\omega_c} + \frac{\alpha^2(n+3)(n+2)(n+1)}{(-3 + 2\xi)\hbar\omega_c}, \quad (12)$$

$$E_n^- = E_n^{0-} - \frac{\alpha^2(n+1)^3}{(1 + 2\xi)\hbar\omega_c} - \frac{\alpha^2 n(n-1)(n-2)}{(-3 + 2\xi)\hbar\omega_c}, \quad (13)$$

where $E_n^{0\pm} = (n + 1/2 \pm \xi)\hbar\omega_c$.

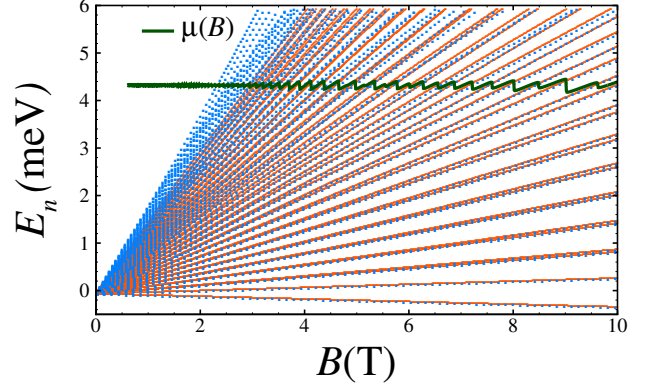


FIG. 1. (Color online) Landau levels of the system evaluated numerically (solid lines) in comparison with those found using Eqs. (12) and (13) (dotted lines) versus magnetic field B . The perturbative Landau levels provided by Eqs. (12) and (13) are in good agreement with the exact numeric ones especially for the lower Landau levels and higher magnetic fields. The oscillating chemical potential is also shown for $n_c = 3.5 \times 10^{16} \text{ m}^{-2}$ showing that the chemical potential depends weakly on B . Here, we use $g = 2$, $\alpha_0 = 5.5 \text{ eV\AA}^3$, $m^* = 1.9 m_e$, $T = 100 \text{ mK}$.

In Fig. 1 we depict the Landau levels of the system obtained numerically (solid lines) in comparison to those found from Eqs. (12) and (13) (dashed lines). We can see that the perturbative Landau levels are in good agreement with the exact ones especially for lower Landau levels and higher magnetic fields. The eigenfunctions, in the first order of perturbation, have also been found as

$$\psi_n^+ = \frac{e^{ik_y y}}{\sqrt{L_y}} N_{n,+} [\phi_n |\uparrow\rangle + C_{n,+} \phi_{n-1} |\downarrow\rangle + D_{n,+} \phi_{n+3} |\downarrow\rangle], \quad (14)$$

$$\psi_n^- = \frac{e^{ik_y y}}{\sqrt{L_y}} N_{n,-} [\phi_n |\downarrow\rangle + C_{n,-} \phi_{n+1} |\uparrow\rangle + D_{n,-} \phi_{n-3} |\uparrow\rangle], \quad (15)$$

where $N_{n,\pm} = 1/\sqrt{1 + C_{n,\pm}^2 + D_{n,\pm}^2}$,

$$C_{n,+} = \alpha n^{3/2}/(1 + 2\xi)\hbar\omega_c,$$

$$D_{n,+} = \left(\frac{\alpha\sqrt{(n+1)(n+2)(n+3)}}{(-3 + 2\xi)\hbar\omega_c} \right) \Theta(n-1),$$

$$C_{n,-} = -\alpha(n+1)^{3/2}/(1 + 2\xi)\hbar\omega_c,$$

$$D_{n,-} = \left(\frac{-\alpha\sqrt{n(n-1)(n-2)}}{(-3 + 2\xi)\hbar\omega_c} \right) \Theta(n-3),$$

and $\Theta(x)$ is the Heaviside function.

Knowing the electron concentration of the system, we can find the field dependent chemical potential of the system through

$$n_c = \int_{-\infty}^{\mu(B)} D(\varepsilon) f(\varepsilon) d\varepsilon, \quad (16)$$

where $f(\varepsilon) = (1 + \exp[\beta(\varepsilon - \mu(B))])^{-1}$ is the Fermi-Dirac distribution and $\beta = 1/k_B T$. The density of states is defined by

$$D(\varepsilon) = 1/A_0 \sum_{n,s,k_y} \delta(\varepsilon - E_n^s), \quad (17)$$

with A_0 is the area of the system. For the sum over k_y , we get $\sum_{k_y} \rightarrow g_s L_y / 2\pi \int_{-L_x/2l_c^2}^{L_x/2l_c^2} dk_y = g_s A_0 / 2\pi l_c^2$. Therefore, Eq. (16) is given by $n_c = 1/2\pi l_c^2 \sum_{n,s} f(E_n^s)$, ($g_s=1$ since the spin degeneracy is lifted in our problem).

Assuming a Landau level broadening of the width Γ [9, 10], we can replace the Delta function of Eq. (17) with a Gaussian and find the density of states as

$$D(\varepsilon) = \frac{g_s}{D_0 \sqrt{2\pi}\Gamma} \sum_{n,s} \exp\left[-\frac{(\varepsilon - E_n^s)^2}{2\Gamma^2}\right], \quad (18)$$

where $D_0 = 2\pi l_c^2$. We will discuss the chemical potential and density of states of the system in more details in Sec. IV.

III. MAGNETOTRANSPORT COEFFICIENTS

In order to find the magnetotransport properties of the system, we follow the approach based on the linear response formalism (as well as the quantum Boltzmann equation) introduced and developed by Van Vilet *et al* in a series of papers [28–31] and then widely applied to 2DEGs in the presence of a perpendicular magnetic field. In this approach, the full Hamiltonian of the system is considered to be composed of a diagonal part, which is the largest part of the Hamiltonian, a nondiagonal interaction part (such as the interaction between electron-impurity or electron-phonon) and finally an external field part, which is the electric field in this case. As a result, the conductivity tensor of the system will have a diagonal as well as a nondiagonal part $\sigma_{\mu\nu} = \sigma_{\mu\nu}^d + \sigma_{\mu\nu}^{nd}$ with $\sigma_{\mu\nu}^d = \sigma_{\mu\nu}^{dif} + \sigma_{\mu\nu}^{col}$. The first term is the usual diffusive current while the second term is the collisional conductivity, which is the many-body contributions of collisions. The diffusive conductivity contains the diagonal elements of the velocity operator, which is zero for both the longitudinal and Hall conductivities. On the other hand, σ_{xx}^{nd} and σ_{yx}^{col} also vanish [30] so that the only terms contributing to the longitudinal and Hall conductivities are $\sigma_{xx} = \sigma_{xx}^{col}$ and $\sigma_{yx} = \sigma_{yx}^{nd}$.

Therefore, the longitudinal conductivity is given by

$$\sigma_{xx}^{col} = \frac{\beta e^2}{A_0} \sum_{\zeta\zeta'} \int d\varepsilon \int d\varepsilon' \delta(\varepsilon - E_\zeta) \delta(\varepsilon' - E_{\zeta'}) \times f(\varepsilon)[1 - f(\varepsilon')] W_{\zeta\zeta'} (x_\zeta - x_{\zeta'})^2, \quad (19)$$

where $|\zeta\rangle = |n, s, k_y\rangle$ and $x_\zeta = \langle \zeta | x | \zeta \rangle$. Considering elastic scattering between carriers and impurities with screened potential of the form $U(\mathbf{r}) = e^2 e^{-k_s r} / 4\pi\epsilon_0\epsilon r$,

we can define the transition rate between state $|\zeta\rangle$ and $|\zeta'\rangle$ as

$$W_{\zeta\zeta'} = \frac{2\pi n_i}{\hbar A_0} \sum_q |U(\mathbf{q})|^2 |F_{\zeta\zeta'}(\mathbf{q})|^2 \delta(\varepsilon - \varepsilon'), \quad (20)$$

where n_i is the impurity density, $F_{\zeta\zeta'} = \langle \zeta | e^{i\mathbf{q}\cdot\mathbf{r}} | \zeta' \rangle$ is the form factor and $U(\mathbf{q}) = e^2 / [2\epsilon_0\epsilon(q^2 + k_s^2)^{1/2}]$ is the Fourier transform of the impurity potential. Here ϵ_0 is the vacuum permittivity, ϵ is the dielectric constant and k_s is the screening wave vector. Since the many-body correlations are suppressed in the presence of the magnetic field, we therefore, consider the Hartree-Fock screening of the system. In order to calculate σ_{xx}^{col} , we should note that the evaluation of $F_{\zeta\zeta'}$ leads to $\delta_{k_y, k_y - q_y}$ and therefore we have $(x_\zeta - x_{\zeta'})^2 = (k_y - k_y')^2 l_c^4 = q^2 \sin^2 \phi l_c^4$. We also have $\sum_{k_y} = A_0 / 2\pi l_c^2$ and $\sum_q \rightarrow A_0 / (2\pi)^2 \int q dq d\phi$. We can once again replace the Delta functions in (19) with a Gaussian to account for level broadening. Performing the integration over ϕ and setting $u = q^2 l_c^2 / 2$, we finally have

$$\sigma_{xx}^{col} = \frac{e^2}{h} \frac{\beta}{2\pi\Gamma^2 l_c^2} n_i U_0^2 \sum_\zeta \int du u |F_\zeta(u)|^2 \times \int d\varepsilon \exp\left[-\frac{(\varepsilon - E_\zeta)^2}{\Gamma^2}\right] f(\varepsilon)[1 - f(\varepsilon)], \quad (21)$$

with $F_\zeta(u) \equiv F_{\zeta\zeta}(u)$ and $U_0 = e^2 / 2\epsilon_0\epsilon k_s$. The above expression is found using the fact that $|F_\zeta(u)|^2 \sim e^{-u}$ (see Appendix. A), the most important contribution to the integral comes from small u and therefore in the denominator of $U(\mathbf{q})$ we can neglect q^2 with respect to k_s . To evaluate the above expression, we should calculate the integrals of the form $I_\zeta = \int u |F_\zeta(u)|^2 du$. In an appropriate condition discussed before, this integral can be evaluated analytically using the approximate eigenvalues and eigenfunctions found in previous section (see Appendix. A). We can estimate the level broadening from $\Gamma_\zeta = \hbar \sum_{\zeta'} W_{\zeta\zeta'}$ without considering the spin-orbit interaction [32] so that we have $\Gamma^2 \approx n_i U_0^2 / \sqrt{2\pi} l_c^2$. We restore the U_0 and k_s in the parameter Γ .

It should be noted that in general case of the electronic mobility of LAO/STO interface, an anisotropic three band Boltzmann equation is needed to find the transport properties of the system [33]. To do so, a three band Hamiltonian with the anisotropic characteristic of the dielectric function might be considered.

Since the time-reversal symmetry is broken, the hall conductivity is nonzero. The Hall conductivity can thus be written as

$$\sigma_{yx}^{nd} = \frac{i\hbar e^2}{A_0} \sum_{\zeta \neq \zeta'} \frac{f(E_\zeta) - f(E_{\zeta'})}{(E_\zeta - E_{\zeta'})(E_\zeta - E_{\zeta'} + i\Gamma_\zeta)} v_{\zeta\zeta'}^y v_{\zeta'\zeta}^x, \quad (22)$$

where $v_{\zeta\zeta'}^y = \langle \zeta | v_y | \zeta' \rangle$ and $v_{\zeta'\zeta}^x = \langle \zeta' | v_x | \zeta \rangle$ are the non-diagonal matrix element of the velocity operator and we assume that $\Gamma_\zeta = \Gamma$. In order to obtain an expression for

the Hall conductivity, we need to have the components of the velocity operator $v_x = \partial H / \partial p_x$ and $v_y = \partial H / \partial p_y$ which read as

$$v_x = \begin{pmatrix} i\gamma(a^\dagger - a) & i\lambda(3a^2 + a^{\dagger 2} - 2a^\dagger a - 1) \\ -i\lambda(3a^{\dagger 2} + a^2 - 2a^\dagger a - 1) & i\gamma(a^\dagger - a) \end{pmatrix}, \quad (23)$$

$$v_y = \begin{pmatrix} \gamma(a^\dagger + a) & \lambda(3a^2 + a^{\dagger 2} + 2a^\dagger a + 1) \\ -\lambda(3a^{\dagger 2} + a^2 + 2a^\dagger a + 1) & \gamma(a^\dagger + a) \end{pmatrix}, \quad (24)$$

with $\gamma = \sqrt{2\hbar m^* \omega_c} / 2$ and $\lambda = \alpha_0 m^* \omega_c / \hbar^2$. The matrix elements of the velocity operator are given in Appendix B for the perturbative regime. We see that the summation over k_y in Eq. (22) gives $A_0 / 2\pi l_c^2$ and also the Kronecker delta appearing in the matrix elements of the velocity operator allows only special values for n' , so considering also δ_{k_y, k'_y} we have $\Sigma_{\zeta \neq \zeta'} \rightarrow \Sigma_{n, ++} + \Sigma_{n, --} + \Sigma_{n, +-} + \Sigma_{n, -+}$, which show both intraband scatterings the same as interband ones.

The resistivity tensor can also be written in terms of the conductivity tensor such that for magnetoresistivity we have $\rho_{xx} = \sigma_{yy} / (\sigma_{xx}\sigma_{yy} - \sigma_{xy}\sigma_{yx})$ and the Hall resistivity is $\rho_{yx} = -\sigma_{yx} / (\sigma_{xx}\sigma_{yy} - \sigma_{xy}\sigma_{yx})$.

IV. RESULTS AND DISCUSSIONS

In this section, we present the numerical results obtained for the magnetotransport properties of a two-band 2DEG with an anisotropic cubic Rashba spin-orbit interaction. An anomalous beating pattern is found in the low magnetic field regime for all quantities reported here involving the chemical potential, density of states and also longitudinal conductivity and resistivity. The beating pattern is the characteristic of systems with two subbands each of which has a different level spacing, so that the energy levels of one subband grows faster than that of the other one. Therefore, the energy level of one subband can sometimes be located in the middle of two energy levels of the other subband creating a node in the density profile. On the other hand, the energy levels of the two subbands can also meet making a maximum in quantum oscillations.

These two subbands are the Rashba spin-split bands in our case. We should note that although even in the absence of the Rashba splitting, the Zeeman term splits the bands into two branches, since the Landau level spacing of both branches is the same, no beating pattern shows up in this case. We can conclude from the perturbed energy levels that the Rashba splitting is proportional to n^3 (n being the Landau level index), so for lower magnetic fields where more Landau levels are occupied, the significant role of Rashba spin splitting leads to the emergence of the beating pattern. As we increase the magnetic field and the higher Landau levels become empty,

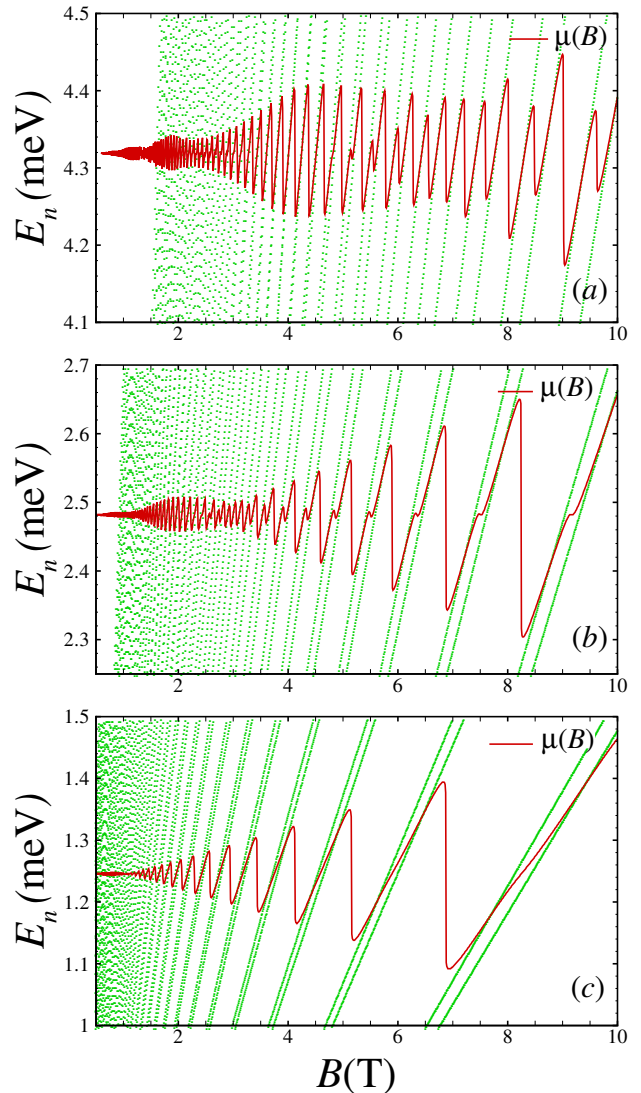


FIG. 2. (Color online) Landau levels (dotted lines) and the chemical potential (solid line) of the system at $T = 100$ mK as functions of magnetic field B for (a) $n_c = 3.5 \times 10^{16} \text{ m}^{-2}$, (b) $n_c = 2 \times 10^{16} \text{ m}^{-2}$ and (c) $n_c = 1 \times 10^{16} \text{ m}^{-2}$. The chemical potential shows a beating pattern in lower magnetic fields specially for higher densities.

the constant Zeeman splitting will be the dominant spin splitting mechanism.

If not otherwise specified, the parameters we used for our calculations are; $g = 2$ [2], $\alpha_0 = 5.5 \text{ eV}\text{\AA}^3$, $m^* = 1.9 m_e$ (m_e being free electron mass) [34] and $n_c = 3.5 \times 10^{16} \text{ m}^{-2}$. The density concentration is chosen such that we can find an appropriate insight to the problem. The same reasoning is also valid for lower densities. To cover a large magnetic field range in our calculations, we have evaluated the magnetotransport properties of the system numerically, since we pointed out earlier that the perturbative expressions are applicable for lower density and higher magnetic field regimes.

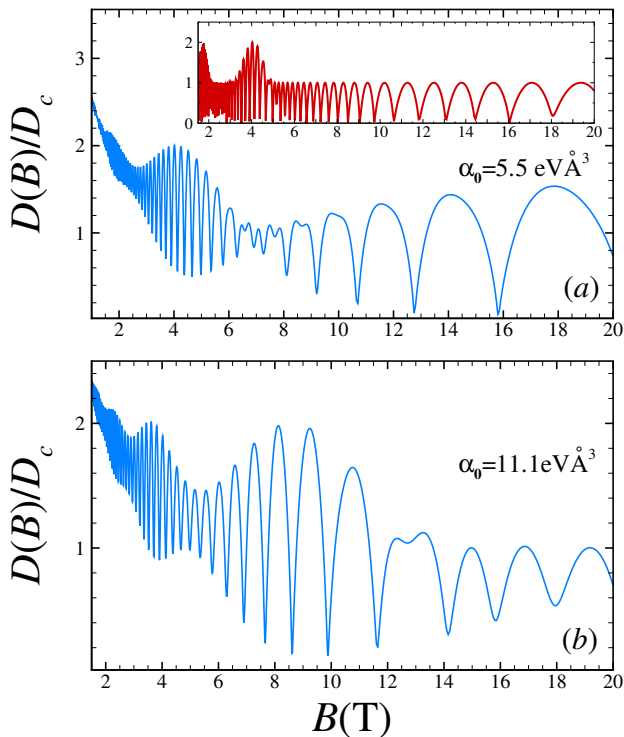


FIG. 3. (Color online) Dimensionless density of states of the system at $T = 100$ mK as a function of magnetic field B for (a) $\alpha_0 = 5.5 \text{ eV}\text{\AA}^3$ and (b) $\alpha_0 = 11.1 \text{ eV}\text{\AA}^3$. Both figures are plotted for $\Gamma = 0.03\sqrt{B}$ meV. Inset: The same as in (a) but with $\Gamma = 0.01\sqrt{B}$ meV.

In Fig. 2, we show the chemical potential of the system for different density concentrations. As expected, a beating pattern can be seen in lower magnetic fields specially for higher densities. This is obvious because the Rashba spin splitting is related to k_F through $\Delta_R = 2\alpha k_F^3 |\cos 2\theta|$. Therefore, in lower densities, Δ_R is too small that the beating pattern appears only in very low magnetic fields.

In Fig. 3, we plot the dimensionless density of states of the system $D(B)/D_c$ for different strengths of the Rashba interaction ($D_c = g_s/D_0\sqrt{2\pi}\Gamma$). We see that the oscillations of Fig. 3(a) follow the same pattern as the chemical potential with the same density. Fig. 3(b) shows the same result for a larger value of α_0 . In this case, the beating pattern persists up to larger magnetic fields with more periods of beatings. As we stated before, the Rashba interaction is responsible for the foundation of the beating pattern so that a stronger Rashba interaction results in beatings, which survives up to larger magnetic fields. The density pattern is illustrated in the inset of Fig. 3(a) for a smaller Landau level broadening. We can see that in this case, the periods of the beatings are not formed completely in the low magnetic field region and the Zeeman spin-split peaks can be distinguished in larger magnetic fields. Furthermore, the piecewise parabolic pattern of the density of states in

terms of the magnetic field at large B , suggests a similar magnetic dependence of the ground-state energy of the system.

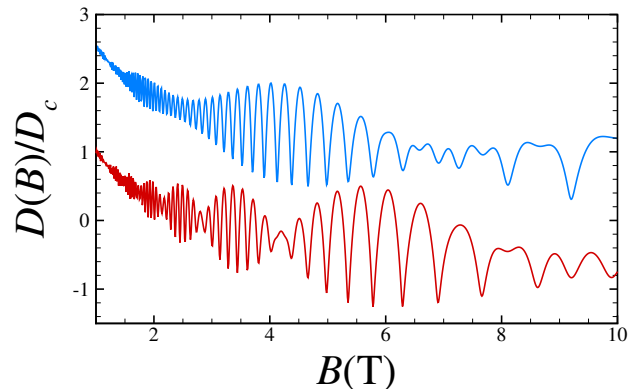


FIG. 4. (Color online) Dimensionless density of states of the system at $T = 100$ mK as a function of the magnetic field B (upper figure) in comparison with that of a system with isotropic k-cubic Rashba interaction (lower figure). Both figures are plotted for $\Gamma = 0.03\sqrt{B}$ meV and $\alpha_0 = 5.5 \text{ eV}\text{\AA}^3$. The lower graph is shifted vertically for clarity.

We compare the density profile of the present system with the one with the isotropic k-cubic Rashba interaction in Fig. 4. The oscillations of the present system in a low magnetic field show a rather anomalous behavior with not the equal number of the peaks in each beating period in comparison with that of the isotropic Rashba one. Such anomalous beating pattern is expected in the systems with anisotropic spin splitting owing to the magnetic break down at the points on the Fermi surface with a smaller spin splitting [35]. In these special points, the electrons can tunnel from one of the Fermi surfaces to another one.

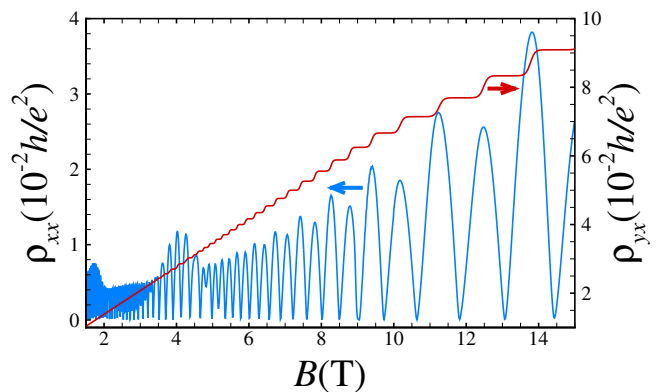


FIG. 5. (Color online) Hall and longitudinal resistivities versus magnetic field B for $T = 50$ mK. The steps between integer quantum Hall plateaus coincide well with the peaks of the longitudinal resistivity. For lower magnetic fields, as the beatings begin to show up in longitudinal resistivity the Hall plateaus also seem to behave in a different way.

The longitudinal and Hall resistivities are plotted in Fig. 5. For evaluation of the longitudinal resistivity the Landau level broadening is assumed to be $\Gamma = 0.01\sqrt{B}$ meV in accordance with the experimental reports finding a much smaller value for Landau level broadening compared to their spacing [8, 11]. The same oscillating pattern (as in Fig. 2(a)) is seen in the longitudinal resistivity of the system. The somehow incomplete beatings persist up to about $B \approx 4.7$ T. As we decrease the density concentration to for example $n_c = 2 \times 10^{16} \text{m}^{-2}$ the beatings disappear for magnetic fields larger than $B \approx 2$ T. We should note that the beating pattern exists in much lower magnetic fields as well, but it is suppressed in this limit due to the Landau level broadening effect. The Hall resistivity versus magnetic field is also shown in this figure. It can be seen that the steps between integer quantum Hall plateaus (in units of h/e^2) coincide well with the sharp peaks of the longitudinal resistivity. For lower magnetic fields, as the beatings begin to show up in the longitudinal resistivity, the Hall plateaus also seem to behave in a different way.

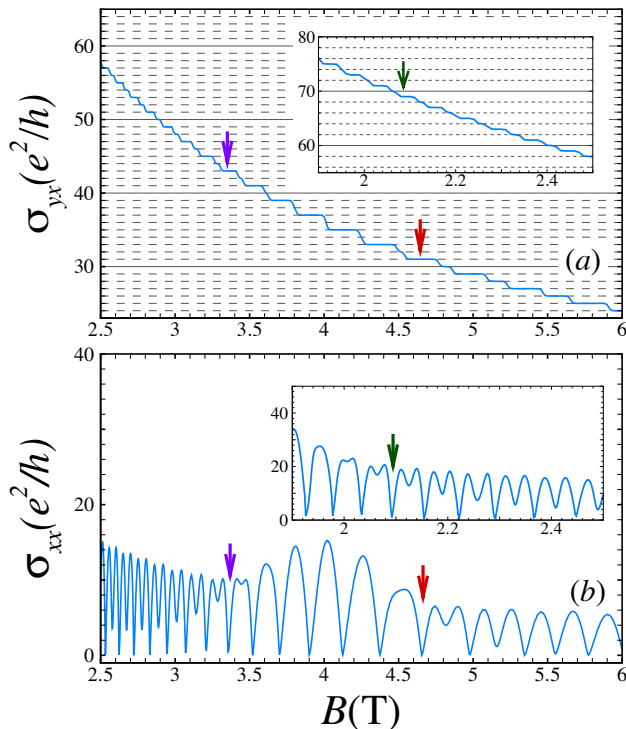


FIG. 6. (Color online) Hall (a) and longitudinal (b) conductivities as functions of magnetic field at $T = 50$ mK. The insets are the same as figures but for lower magnetic field. The arrows show the onsets of the changes in the behavior of the graphs.

In order to better understand the phenomenon, we concentrate on a weak magnetic field regime in Fig. 6, where we plot the longitudinal conductivity in Fig. 6(a) as well as the Hall conductivity of the same system in Fig. 6(b) with insets in both figures illustrating the lower magnetic

field calculations. The interesting point about the Hall conductivity plateaus (plotted in units of e^2/h) is that decreasing the magnetic field and moving from spin-split peaks to the beating regime in longitudinal conductivity figure at $B \approx 4.7$ T, the Hall plateaus also change in a way that the integer Hall plateaus (with both even and odd filling factors) are replaced by the odd ones. The reverse phenomenon can be traced at $B \approx 3.4$ T and once more at $B \approx 2.1$ T the same process begins. When the Landau levels of two branches of the system are far enough from each other, both odd and even plateaus can be distinguished in the system, but as the magnetic field is decreased, the diverse growing rate of Landau level energies with respect to the filling factor leads to the condition where two subband energies approach each other and in a region where they are so close, we will have spin degenerate levels with only odd filling factors. For example at $B \approx 2.5$ T where we expect an even Hall plateau, the energy difference between adjacent Landau levels is about 0.014 meV with Landau level broadening being $\Gamma \approx 0.021$ meV. The interplay between large broadening and small level splitting results in the disappearance of the Hall plateau. As we lower the magnetic field the same approach is repeated. Note that for the spin-split peaks to appear in SdH oscillations (as well as even-odd filling factors), we need a small Landau level broadening and low-temperature condition.

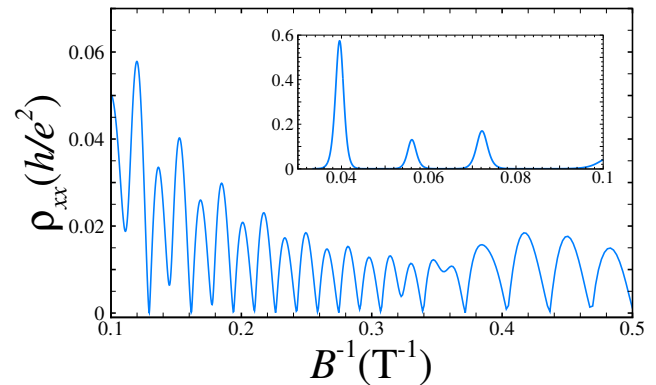


FIG. 7. (Color online) Magnetoresistivity as a function of B^{-1} for $n_c = 1.5 \times 10^{16} \text{m}^{-2}$, $\alpha_0 = 11.1 \text{eV}\text{\AA}^3$ and $T = 50$ mK. Inset: The same as in figure but for larger magnetic fields

To compare our results with SdH experiments, we plot the magnetoresistivity of the system versus $1/B$ in Fig. 7. The figure is plotted for $T = 100$ mK, $\Gamma = 0.01\sqrt{B}$ meV, $\alpha_0 = 11.1 \text{eV}\text{\AA}^3$ and $n_c = 1.5 \times 10^{16} \text{m}^{-2}$ in accordance with the densities reported in experiments. The inset figure also shows the high field magnetoresistivity. The oscillation pattern in this figure is qualitatively consistent with that observed in the experiments especially at larger magnetic fields [9–11]. We should note that the smallest magnetic field for which the SdH oscillations have been observed in the present system is about 2 T. As we stated before for low density regime the beatings occur in lower

magnetic fields, which is due to a small Landau level separation in the present system, it is not easy to be detected in experiments.

It is also interesting to trace the magneto-oscillations of the system in the analogous de Haas-van Alphen oscillations, which are the oscillations of the magnetization of the electron gas defined as

$$M = -\frac{\partial F}{\partial B}\Big|_{n_c, T}, \quad (25)$$

where

$$F(T) = \int d\varepsilon D(\varepsilon) \{ \varepsilon f(\varepsilon) + k_B T [f(\varepsilon) \ln(f(\varepsilon)) + (1 - f(\varepsilon)) \ln(1 - f(\varepsilon))] \}, \quad (26)$$

is the free energy per unit area at temperature T . In Fig. 8(a) we illustrate the free energy of the system as a function of magnetic field for different temperatures. The oscillations of the free energy also follow the oscillations in the chemical potential, although it is hard to be resolved especially for higher temperatures. These oscillations are more clear in magnetization shown in Fig. 8(b). The free energy exhibits kinks and the magnetization has jumps at those values of the magnetic field, where a Landau level becomes completely empty. The parameters in this figure are the same as in Fig. 3(a) and we can see the same pattern in the magnetization oscillations as well.

V. CONCLUDING REMARKS

We have numerically evaluated the magnetotransport coefficients of the 2DEG at the interface of LaAlO₃ and SrTiO₃. A perturbative approach is also suggested, which could be used for lower densities and not very small magnetic fields. We have also discussed the role of the anisotropic k-cubic Rashba spin splitting as well as the Zeeman splitting. A beating pattern is found in low magnetic field regime caused by the presence of Rashba term in the Hamiltonian. The somehow anomalous nature of beatings in comparison with beatings caused by isotropic k-cubic Rashba interaction is illustrated. The impact of physical characteristics of the system such as the Landau level broadening Γ , Rashba constant α_0 and electron concentration n_c is considered as well. We have found that the beating pattern persists up to larger magnetic fields for higher densities and also stronger Rashba interactions. The Hall plateaus of the system are also plotted and the expected coincidence of the steps between plateaus in the Hall resistivity with the peaks of the longitudinal resistivity is shown.

A quantitative agreement between the SdH oscillations in our model with the experimental reports is found for somehow larger magnetic fields and low electron densities. We would like to emphasize that the hallmark of

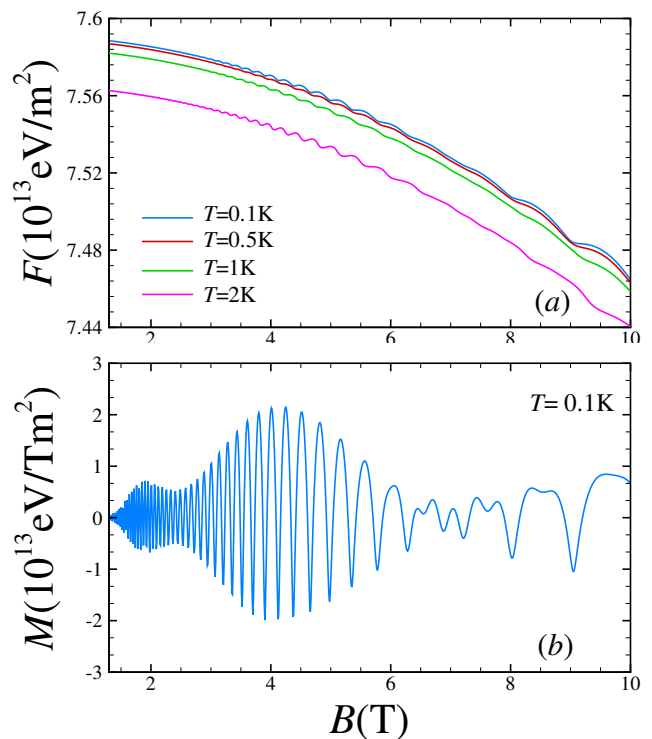


FIG. 8. (Color online) (a) Free energy of the system F versus the magnetic field B for different temperatures. (b) Magnetization oscillations M versus magnetic field B at $T = 100$ mK. We consider $n_c = 3.5 \times 10^{16} \text{ m}^{-2}$, $\alpha_0 = 5.5 \text{ eV}\text{\AA}^3$ and $\Gamma = 0.03\sqrt{B} \text{ meV}$.

our model is the appearance of a peculiar beating pattern in low magnetic fields, which can not be detected in low-density regime, according to our calculations. On the other hand for quantum oscillations to be observed, the condition $\hbar\omega_c > k_B T$ should be fulfilled and due to the larger effective mass in the present system in comparison with conventional 2DEGs, lower temperatures for detecting the SdH oscillations and Hall plateaus in the typical ranges of magnetic fields is essential.

VI. ACKNOWLEDGEMENTS

R. A would like to thank the international center of theoretical physics, ICTP, Italy where the final stage of this work has been completed. This work is supported by the Iran Science Elites Federation grant no 11/66332.

Appendix A

Using the approximate eigenvalues and eigenfunctions (12)-(15) we can obtain the following expressions for $|F_n^+(u)|^2$ and $|F_n^-(u)|^2$

$$\begin{aligned}
|F_n^+(u)|^2 &= |\langle \psi_n^+ | e^{i\mathbf{q}\cdot\mathbf{r}} | \psi_n^+ \rangle|^2 \\
&= e^{-u} N_{n,+}^4 [L_n(u) + C_{n,+}^2 L_{n-1}(u) + D_{n,+}^2 L_{n+3}(u) \\
&\quad + 2\sqrt{(n-1)!/(n+3)!} C_{n,+} D_{n,+} u^2 L_{n-1}^{(4)}(u)]^2 \delta_{k_y, k'_y + q_y}, \tag{A1}
\end{aligned}$$

$$\begin{aligned}
|F_n^-(u)|^2 &= |\langle \psi_n^- | e^{i\mathbf{q}\cdot\mathbf{r}} | \psi_n^- \rangle|^2 \\
&= e^{-u} N_{n,-}^4 [L_n(u) + C_{n,-}^2 L_{n+1}(u) + D_{n,-}^2 L_{n-3}(u) \\
&\quad + 2\sqrt{(n-3)!/(n+1)!} C_{n,-} D_{n,-} u^2 L_{n-3}^{(4)}(u)]^2 \delta_{k_y, k'_y + q_y}, \tag{A2}
\end{aligned}$$

Here $L_n^{(m)}$ is the generalized Laguerre polynomial and as defined before $u = q^2 l_c^2 / 2$. After a lengthy calculation we find the following expressions for I_n^+ and I_n^-

$$\begin{aligned}
\frac{I_n^+}{N_{n,+}^4} &= (2n+1) + C_{n,+}^4 (2n-1) + D_{n,+}^4 (2n+7) \\
&\quad + 4C_{n,+}^2 D_{n,+}^2 (2n+3) - C_{n,+}^2 n + 12 \frac{C_{n,+} D_{n,+}}{N_{n,+}^2} \sqrt{\frac{(n-1)!}{(n+3)!}}, \tag{A3}
\end{aligned}$$

$$\begin{aligned}
\frac{I_n^-}{N_{n,-}^4} &= (2n+1) + C_{n,-}^4 (2n+3) + D_{n,-}^4 (2n-5) \\
&\quad + 4C_{n,-}^2 D_{n,-}^2 (2n-1) - C_{n,-}^2 (n+1) + 12 \frac{C_{n,-} D_{n,-}}{N_{n,-}^2} \sqrt{\frac{(n-3)!}{(n+1)!}}, \tag{A4}
\end{aligned}$$

Appendix B

The matrix elements of the velocity operator read as

$$\begin{aligned}
\langle \psi_n^+ | v_y | \psi_{n'}^+ \rangle &= -i \langle \psi_n^+ | v_x | \psi_{n'}^+ \rangle = \delta_{k_y k'_y} (N_{n,+} N_{n',+}) \times \\
&\{ (D_{n,+} B_1) \delta_{n',n+5} + (A_1 + D_{n,+} B_2) \delta_{n',n+3} + (A_2 + C_{n,+} B_1 + D_{n,+} B_3) \delta_{n',n+1} \\
&\quad + (A_3 + C_{n,+} B_2 + D_{n,+} B_4) \delta_{n',n-1} + (A_4 + C_{n,+} B_3) \delta_{n',n-3} + (A_5 + C_{n,+} B_4) \delta_{n',n-5} \}, \tag{B1}
\end{aligned}$$

$$\begin{aligned}
\langle \psi_n^- | v_y | \psi_{n'}^+ \rangle &= -i \langle \psi_n^- | v_x | \psi_{n'}^+ \rangle = \delta_{k_y k'_y} (N_{n,-} N_{n',+}) \times \\
&\{ (C_{n,-} A_1) \delta_{n',n+4} + (C_{n,-} A_2 + B_1) \delta_{n',n+2} + (D_{n,-} A_1 + C_{n,-} A_3 + B_2) \delta_{n',n} \\
&\quad + (D_{n,-} A_2 + C_{n,-} A_4 + B_3) \delta_{n',n-2} + (D_{n,-} A_3 + C_{n,-} A_5 + B_4) \delta_{n',n-4} + (D_{n,-} A_4) \delta_{n',n-6} + (D_{n,-} A_5) \delta_{n',n-8} \}, \tag{B2}
\end{aligned}$$

where the constants A_i and B_i have different values for $\langle \psi_n^+ | v_y | \psi_{n'}^+ \rangle$ and $\langle \psi_n^+ | v_x | \psi_{n'}^+ \rangle$ such that $A_1 = 3\lambda C_{n',+} \sqrt{n'-1} \sqrt{n'-2}$, $A_2 = \pm \gamma \sqrt{n'} \pm \lambda C_{n',+} (2n'-1)$, $A_3 = \gamma \sqrt{n'+1} + \lambda C_{n',+} \sqrt{n'} \sqrt{n'+1} + 3\lambda D_{n',+} \sqrt{n'+3} \sqrt{n'+2}$, $A_4 = \pm \lambda D_{n',+} (2n'+7)$,

$A_5 = \lambda D_{n',+} \sqrt{n'+5} \sqrt{n'+4}$, $B_1 = -\lambda \sqrt{n'} \sqrt{n'-1} \pm \gamma C_{n',+} \sqrt{n'-1}$, $B_2 = \mp \lambda (2n'+1) + \gamma C_{n',+} \sqrt{n'}$, $B_3 = -3\lambda \sqrt{n'+2} \sqrt{n'+1} \pm \gamma D_{n',+} \sqrt{n'+3}$ and $B_4 = \gamma D_{n',+} \sqrt{n'+4}$. All the upper signs correspond to $\langle \psi_n^+ | v_y | \psi_{n'}^+ \rangle$ and the lower signs correspond to $\langle \psi_n^+ | v_x | \psi_{n'}^+ \rangle$.

In the same way we will have

$$\begin{aligned}
\langle \psi_n^- | v_y | \psi_{n'}^- \rangle &= -i \langle \psi_n^- | v_x | \psi_{n'}^- \rangle = \delta_{k_y k'_y} (N_{n,-} N_{n',-}) \times \\
&\{ (C_{n,-} A_1 + B_1) \delta_{n',n+5} + (C_{n,-} A_2 + B_2) \delta_{n',n+3} + (D_{n,-} A_1 + C_{n,-} A_3 + B_3) \delta_{n',n+1} \\
&\quad + (D_{n,-} A_2 + C_{n,-} A_4 + B_4) \delta_{n',n-1} + (D_{n,-} A_3 + B_5) \delta_{n',n-3} + (D_{n,-} A_4) \delta_{n',n-5} \}, \tag{B3}
\end{aligned}$$

$$\begin{aligned}
\langle \psi_n^+ | v_y | \psi_{n'}^- \rangle &= -i \langle \psi_n^+ | v_x | \psi_{n'}^- \rangle = \delta_{k_y k'_y} (N_{n,+} N_{n',-}) \times \\
&\{ (D_{n,+} B_1) \delta_{n',n+8} + (D_{n,+} B_2) \delta_{n',n+6} + (A_1 + C_{n,+} B_1 + D_{n,+} B_3) \delta_{n',n+4} \\
&\quad + (A_2 + C_{n,+} B_2 + D_{n,+} B_4) \delta_{n',n+2} + (A_3 + C_{n,+} B_3 + D_{n,+} B_5) \delta_{n',n} + (A_4 + C_{n,+} B_4) \delta_{n',n-2} + (C_{n,+} B_5) \delta_{n',n-4} \}, \tag{B4}
\end{aligned}$$

With $A_1 = \pm \gamma D_{n',-} \sqrt{n'-3}$, $A_2 = \gamma D_{n',-} \sqrt{n'-2} + 3\lambda \sqrt{n'} \sqrt{n'-1}$, $A_3 = \pm \gamma C_{n',-} \sqrt{n'+1} \pm \lambda (2n'+1)$,

$$A_4 = \gamma C_{n',-} \sqrt{n'+2} + \lambda \sqrt{n'+2} \sqrt{n'+1}, \quad B_1 = -3\lambda D_{n',-} \sqrt{n'-2} \sqrt{n'-1} - \lambda C_{n',-} \sqrt{n'+1} \sqrt{n'} \pm \gamma \sqrt{n'},$$

$$\lambda D_{n',-} \sqrt{n'-3} \sqrt{n'-4}, \quad B_2 = \mp \lambda D_{n',-} (2n' - 5), \quad B_3 = \gamma \sqrt{n'+1} \mp \lambda C_{n',-} (2n' + 3) \quad \text{and} \quad B_5 = -3\lambda C_{n',-} \sqrt{n'+3} \sqrt{n'+2}.$$

-
- [1] S. Thiel, G. Hammerl, A. Schmehl, C. W. Schneider and J. Mannhart, *Science* **313**, 1942 (2006).
- [2] A. D. Caviglia, M. Gabay, S. Gariglio, N. Reyren, C. Cancellieri, and J.-M. Triscone, *Phys. Rev. Lett.* **104**, 126803 (2010).
- [3] A. Brinkman, M. Huijben, M. van Zalk, J. Huijben, U. Zeitler, J. C. Maan, W. G. van der Wie, G. Rijnders, D. H. A. Blank and H. Hilgenkamp, *Nat. Mater.* **6**, 493, (2007)
- [4] N. Reyren, S. Thie, A. D. Caviglia, L. Fitting Kourkoutis, G. Hammer, C. Richter, C. W. Schneider, T. Kopp, A.S. Rüetschi, D. Jaccard, M. Gabay, D. A. Muller, J.M. Triscone and J. Mannhart, *Science* **317**, 1196 (2007).
- [5] D. A. Dikin, M. Mehta, C. W. Bark, C. M. Folkman, C. B. Eom and V. Chandrasekhar, *Phys. Rev. Lett.* **107**, 056802 (2011).
- [6] Y.-Y. Pai, A. Tylan-Tyler, P. Irvin, and J. Levy, *Rep. prog. phys.* **81**, 036503 (2018).
- [7] A. D. Caviglia, S. Gariglio, C. Cancellieri, B. Sacepe, A. Fête, N. Reyren, M. Gabay, A. F. Morpurgo and J. M. Triscone, *Phys. Rev. Lett.* **105**, 236802 (2010).
- [8] M. Ben Shalom, A. Ron, A. Palevski and Y. Dagan, *Phys. Rev. Lett.* **105**, 206401 (2010).
- [9] A. Fête, S. Gariglio, C. Berthod, D. Li, D. Stornaiuolo, M. Gabay and J.M. Triscone, *N. J. Phys.* **16**, 112002 (2014).
- [10] M. Yang, K. Han, O. Toressin, M. Pierre, S. W. Zeng, Z. Huang, T. V. Venkatesan, M. Goiran, J. M. D. Coey, Ariando and W. Escoffier, *Appl. Phys. Lett.* **109**, 122106 (2016).
- [11] Y. Xie, C. Bell, M. Kim, H. Inoue, Y. Hikita and H. Y. Hwang, *Solid State Communications* **197**, 25 (2014).
- [12] F. Trier, G. E. D. K. Prawiroatmodjo, Z. Zhong, D. V. Christensen, M. vonSoosten, A. Bhowmik, JuanMaria-Garcia Lastra, Y. Chen, T. S. Jespersen, N. Pryds, *Phys. Rev. Lett.* **117**, 096804 (2016).
- [13] P. K. Rout, I. Agireen, E. Maniv, M. Goldstein, and Y. Dagan, *Phys. Rev. B* **95**, 241107 (2017).
- [14] N. Reyren, M. Bibes, E. Lesne, J. M. George, C. Deranlot, S. Collin, A. Barthélémy, H. Jaffrés, *Phys. Rev. Lett.* **108**, 186802 (2012).
- [15] R. Pentcheva and W. E. Pickett, *Phys. Rev. B* **74**, 035112 (2006).
- [16] Z. S. Popović, S. Satpathy and R.M. Martin, *Phys. Rev. Lett.* **101**, 256801 (2008).
- [17] G. Khalsa, B. Lee and A. H. MacDonald, *Phys. Rev. B* **88**, 041302 (2013).
- [18] Y. Kim, R. M. Lutchyn and C. Nayak, *Phys. Rev. B* **87**, 245121 (2013).
- [19] J. Zhou, W.-Y. Shan and D. Xiao, *Phys. Rev. B* **91**, 241302 (2015).
- [20] Z. Zhong, A. Tóth and K. Held, *Phys. Rev. B* **87**, 161102 (2013).
- [21] K. V. Shanavas, *Phys. Rev. B* **93**, 045108 (2016).
- [22] H. Nakamura, T. Koga and T. Kimura, *Phys. Rev. Lett.* **108**, 206601 (2012).
- [23] H. Liang, L. Cheng, L. Wei, Z. Luo, G. Yu, C. Zeng and Z. Zhang, *Phys. Rev. B* **92**, 075309 (2015).
- [24] X. F. Wang and P. Vasilopoulos, *Phys. Rev. B* **67**, 085313 (2003).
- [25] M. Zarea and S. E. Ulloa, *Phys. Rev. B* **72**, 085342 (2005).
- [26] M. Zarea and S. E. Ulloa, *Phys. Rev. B* **73**, 165306 (2006).
- [27] A. Mawrie, T. Biswas and T. K. Ghosh, *J. Phys.: Condens. Matter* **26**, 405301 (2014).
- [28] K. M. Van Vliet, *J. Math. Phys.* **19**(6), 1345 (1978).
- [29] K. M. Van Vliet, *J. Math. Phys.* **20**(12), 2573 (1979).
- [30] M. Charbonneau, K. M. Van Vliet and P. Vasilopoulos, *J. Math. Phys.* **23**(2), 318 (1982)
- [31] P. Vasilopoulos and C. M. Van Vliet, *J. Math. Phys.* **25**(5), 1391 (1984)
- [32] P. Vasilopoulos and C. M. Van Vliet, *Phys. Rev. B* **34**, 1057 (1986).
- [33] A. Faridi, R. Asgari and A. Langari, *Phys. Rev. B* **93**, 235306 (2016).
- [34] m^* and α_0 are evaluated from their definitions in Ref. 19 with numerical values adapted from Ref. 20
- [35] E. A. de Andrada e Silva, G. C. La Rocca and F. Bassani, *Phys. Rev. B* **50**, 8523 (1994).